university of groningen

University Medical Center Groningen

University of Groningen

Structure and domain formation in ferroelectric thin films

Vlooswijk, Ard H.G.

IMPORTANT NOTE: You are advised to consult the publisher's version (publisher's PDF) if you wish to cite from it. Please check the document version below.

Document Version
Publisher's PDF, also known as Version of record

Publication date:
2009

Link to publication in University of Groningen/UMCG research database

Citation for published version (APA):
Vlooswijk, A. H. G. (2009). *Structure and domain formation in ferroelectric thin films*. [Thesis fully internal (DIV), University of Groningen]. [s.n.].

Copyright
Other than for strictly personal use, it is not permitted to download or to forward/distribute the text or part of it without the consent of the author(s) and/or copyright holder(s), unless the work is under an open content license (like Creative Commons).

The publication may also be distributed here under the terms of Article 25fa of the Dutch Copyright Act, indicated by the "Taverne" license. More information can be found on the University of Groningen website: https://www.rug.nl/library/open-access/self-archiving-pure/taverne-amendment.

Take-down policy
If you believe that this document breaches copyright please contact us providing details, and we will remove access to the work immediately and investigate your claim.

Downloaded from the University of Groningen/UMCG research database (Pure): http://www.rug.nl/research/portal. For technical reasons the number of authors shown on this cover page is limited to 10 maximum.

Download date: 15-03-2025

Chapter 6

Ferroelectric nanostructures

Parts of this chapter are submitted as:
W. van Zoelen, A.H.G. Vlooswijk A. Ferri, A.-M. Andringa, B. Noheda and G. ten Brinke – "Ordered arrays of ferroelectric nanoparticles by pulsed laser deposition on PS-*b*-P4VP(PDP) supramolecules-based templates" to *ACS Nano*.

6.1 Introduction

Two types of nanometer-sized structures will be described in this chapter: superlattices and chains of nanodots. Although quite different in appearance, the interest in this kind of structures has a shared origin: in both cases the dimensionality of the ferroelectric is decreased and therefore the interfaces potentially play an important role.

The chains of nanometer-sized $PbTiO_3$ dots are fabricated using spontaneously microphase separated block copolymers. The length scale of 10-100 nm in these microphase separated structures of block copolymers, makes them ideal candidates as templates for the production of nanoscale materials. The diameter of the $PbTiO_3$ nanodots that we have fabricated using these ordered block copolymers is approximately 50 nm, similar to other reports by different methods [139], but still far above the theoretically determined sizes for which size effects strongly influence the objects' properties (~ 6 nm) [140]. Despite the fact that the reduced dimensionality is not expected to play a role at these relatively large sizes, the fabrication and properties of these nanodots can be of interest for applications. After all, the large amount of materials' surface can enhance the influence of the depolarizing field and suppress ferroelectricity, an effect often encountered in applications. By studying such systems, more insight in the role of the depolarizing field can be obtained.

In the case of $PbTiO_3/SrTiO_3$-superlattices, there is only one reduced dimension, the thickness, which implies that these superlattices allow to study

the critical thickness for ferroelectricity. The limited layer thickness of each separate superlattice layer can be tuned to the critical thickness for ferroelectricity to investigate this critical thickness. Moreover, the artificial stacking of alternating $PbTiO_3$ and $SrTiO_3$ layers can induce coupling between the ferroelectric $PbTiO_3$ and the quantum paraelectric $SrTiO_3$ and give rise to enhanced ferroelectric response [141]. The only literature reports of $PbTiO_3$/ $SrTiO_3$ superlattices up to now, have used rf-sputtering [156] or MBE [157] as a growth technique. We use a PLD method in which part of the $SrTiO_3$ is grown as a capping layer of the $PbTiO_3$ and part is grown at increased temperature (790°C). In this way, we prevent Pb loss, yet we are able to grow non-conductive $SrTiO_3$.

6.2 Chains of $PbTiO_3$ nanodots

6.2.1 Introduction

Over the last years a lot of theoretical research has been done concerning the size and shape dependent properties of ferroelectrics at the nanoscale, not only because of the promising technological applications, but also to gain more understanding of the ferroelectric behavior at the nanoscale. Important progress has been achieved in understanding the crucial role of depolarizing fields in nanometer-sized objects, such as nanorods, nanodisks and nanodots [140, 142, 143, 144, 145, 146]. This interest for ferroelectric materials, both for applications and from a fundamental point of view, has given rise to experimental studies of differently shaped ferroelectrics [134, 138, 147, 148].

On the one side, lithography and focused ion beam (FIB) techniques are used to shape bulk or thin film ferroelectrics to a desired shape [52]. On the other side, chemical routes are used to obtain nano-particles of ferroelectrics [149]. Both techniques have their drawbacks: lithography and FIB are expensive and time consuming, and the minimum lateral size is limited to 70-100 nm [150]; macroscopic measurements are usually hard to conduct for nano-objects obtained via chemical routes because of the lack of ordering on a substrate and the small amount of available material.

We use a combination of self-assembly and pulsed laser deposition (PLD) in order to obtain a large number of ordered chains of ~ 50 nm ferroelectrics on a substrate surface. This approach allows the study of the properties

of single ferroelectric nano-objects with atomic force microscopy combined with piezoresponse measurements (p-AFM), while at the same time, the large number of nano-objects available on a single substrate allow macroscopic measurements such as X-ray diffraction (XRD). The technique we have used, bears resemblance with the NSL (nanosphere lithography) approach reported by Ma et al. who used PLD on ordered latex particles to create nano-objects of ferroelectric $BaTiO_3$, however, the nanostructures obtained in our study are one order of magnitude smaller [151].

6.2.2 Experimental

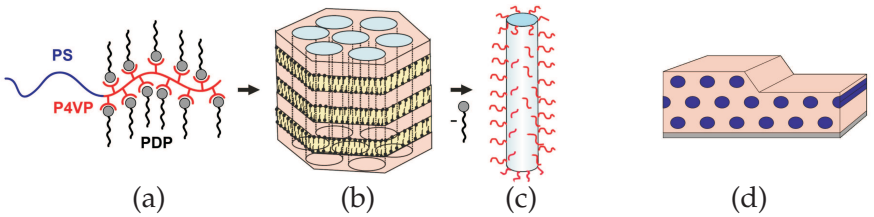

Figure 6.1: Schematic representation of (a) PS-*b*-P4VP(PDP) supramolecule, (b) microphase separated into structures within structures, in this case cylinders-within-lamellae. (c)Nanorod with a PS core and P4VP corona obtained by removal of the PDP from the bulk. (d)PS-*b*-P4VP(PDP) thin film after solvent annealing, forming terraces of parallelly oriented PS cylinders in a P4VP(PDP) matrix.

We have used PS-*b*-P4VP(PDP) comb-shaped supramolecules as depicted in Figure 6.1a as a nano-template to fabricate chains of $PbTiO_3$ nanodots. PS-*b*-P4VP is schematically represented in Figure 6.1a: It is a heteropolymer of polystyrene and poly(4-vinylpyridine) (PS-b-P4VP), with the P4VP hydrogen bonded with pentadecylphenol (PDP). The supramolecules can microphase separate into structures-within-structures, in this case cylinders-within-lamellae as schematically represented in Figure 6.1b. Removal of PDP from a bulk sample results in nanorods with a PS core and a P4VP corona (Figure 6.1c). By spin-coating from a chloroform solution and subsequently annealing the solvent, a PS-*b*-P4VP(PDP) thin film of ovally shaped cylinders remains, forming terraces of paralelly oriented PS cylinders in a P4VP(PDP) matrix (Figure 6.1d; the orientation of P4VP(PDP) lamellae forming the small length scale is not depicted). Washing away PDP also removes the top layer

of cylinders from the film, while a single layer of PS-*b*-P4VP nanorods remains at the interface due to the strong interactions with P4VP (Figure 6.2b).

Previously, these kinds of polymer structures have been made on SiO_2

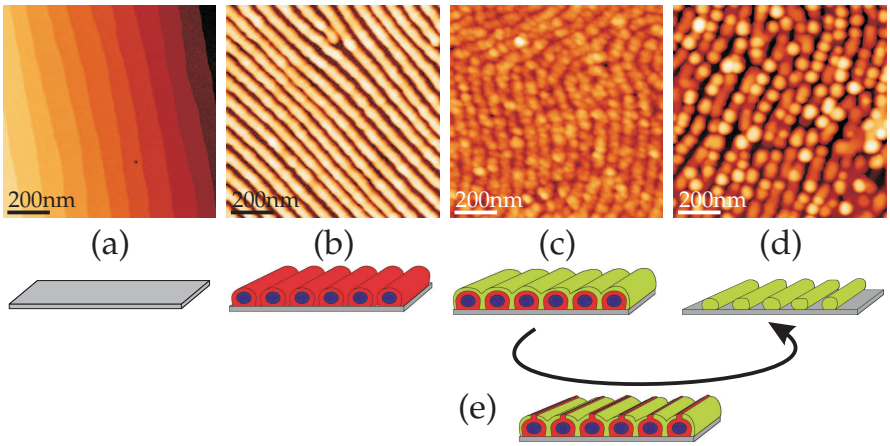

Figure 6.2: a) $SrTiO_3$ substrate with 95 ± 5 nm wide terraces; full z-scale Δz=6 nm. b) P4VP nanorod structure on $SrTiO_3$; Δz=28 nm. c) The same structure as b) covered with amorphous $PbTiO_3$ with a grain-structure deposited by room temperature PLD; Δz=36 nm. d) The same structure as c) after annealing at 565°; Δz=53 nm. In b), c) and d), Fast Fourier Transforms of the image show that the structure is repeating every 65 ± 5 nm. e) During heating the nanorods are degraded and the $PbTiO_3$ crystallizes in such a way that nanostructured $PbTiO_3$ remains.

substrates, but this procedure works equally well on $SrTiO_3$ substrates [152]. This allows us to use $SrTiO_3$ substrates covered with a single layer of oriented block-copolymer cylinders as a growth template. In order to conduct piezoresponse-AFM measurements, we have deposited a conducting bottom electrode of $SrRuO_3$ before coverage with the block-copolymer. Figure 6.2 shows the characteristic AFM images and schematic representations of the different procedure steps for nanorods prepared on $SrTiO_3$. The chemical and thermal treatment of $SrTiO_3$ (001) substrates, as described in chapter 3, leads to a single TiO_2-terminated surface with unit cell steps (Figure 6.2(a)). These substrates have been coated with an ~ 80 nm thin film of comb-shaped supramolecules of polystyrene-block-poly(4-vinylpyridine) (PS-*b*-P4VP) hydrogen bonded with pentadecylphenol (PDP) by spin-coating from a chloroform solution, and subsequently annealed in solvent vapor, which led to

the formation of terraces of parallelly oriented PS cylinders in a matrix of the P4VP(PDP) comb. Subsequent treatment with ultrasound in ethanol, a good solvent for PDP as well as for P4VP, and a non-solvent for PS, separated the rods from each other, removing the top layers of cylinders, while the bottom layer firmly remained at the substrate interface due to strong interactions with P4VP. This resulted in patterned nanorods with a typical height of ~ 25 nm and ~ 65 nm periodicity (Figure 6.2(b)). The distance between the nanorods is hard to measure due to tip convolution effects, but assuming equal densities for all phases, it can be estimated to be 20 nm. The shape of the nanorods is oval-like due to the collapse of the cylindrical structure after swelling.

Due to the low melting point of the polymers, PLD had to be performed at room temperature, coating the patterned nanorods with a continuous layer of ~ 30 nm of amorphous $PbTiO_3$ (with a small Pb-excess) (Figure 6.2(c)). Post-deposition crystallization was carried out at 565°C. This crystallization temperature lies far above the degradation temperature of the nanorods, which start to degrade at ~ 300°C and are evaporated at ~ 450°C as determined by thermogravimetric analysis of pure block copolymer (heating rate = 10°C/min). However, during the degradation of the nanorods, the nanostructures are transferred to the $PbTiO_3$ layer (Figure 6.2(d)). The grain-like structure, which is inherent to room temperature growth of $PbTiO_3$, is not lost upon annealing, although the grain size increases from ~ 30 nm to ~ 50 nm. In the range of 30-120 min annealing time, no effect of the timing on the grain structure has been observed for an annealing temperature of 565°C. Higher annealing temperatures, however, lead to further enlarged grains and the loss of the ordered structure. The mechanism we propose for the transfer of the nanorod shape from P4VP to $PbTiO_3$ is that the P4VP evaporates through the crystallizing $PbTiO_3$ layer and the $PbTiO_3$ preferentially crystallizes on places where it is in contact with the crystalline substrate. In principle, this leads to an inverted nanorod structure: the $PbTiO_3$ crystallizes where there is no nanorod, and it does not where there is nanorod. But due to the morphology, one cannot distinguish the direct versus the inverted structure.

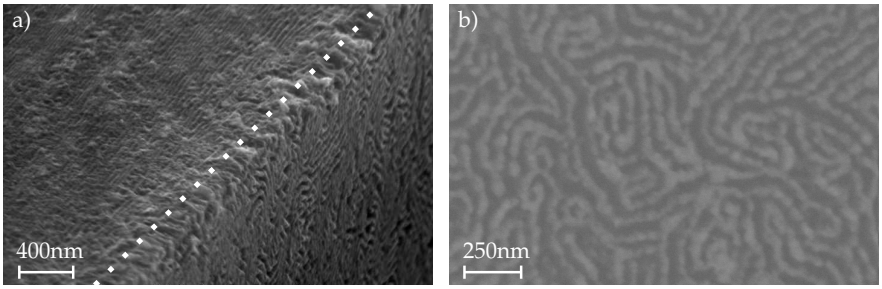

Figure 6.3: SEM images of chains of $PbTiO_3$ nanodots on $SrTiO_3$. a) is a cross-sected sample with the cross-section on the left side of the dotted line and the top surface of the sample on the right. The top surface consists of separated chains, while the cleavage of the $SrTiO_3$ crystal planes can be observed on the left side. b) The difference in electron density between the uncovered surface and the surface covered with chains can be observed in this backscatter electron mode SEM image.

6.2.3 Results and discussion

$PbTiO_3$ morphology

As described in the previous paragraph and shown in Figure 6.2, we can monitor the morphology of the nanorods and -dots by AFM. During the different stages of the process, the periodic chains have a period of approximately 65 nm. But what is more crucial and only limitedly imaged by AFM, is the separation between the rods. The rods seem separated, but due to the finite tip size and nanometer-size of the rods and chains, our AFM measurements are not conclusive concerning the separation or contact between the chains. Although not 100% conclusive, the actual separation of the chains of $PbTiO_3$ nanodots is supported by Figure 6.3(a) which shows the scanning electron micrograph (SEM) of a cross-sected sample.
In addition to this confirmation of the morphology, SEM provides qualitative information on the thin film composition. Figure 6.3(b) clearly shows contrast in a backscattered electron (BSE) mode SEM image. This proves that regions with a higher and lower average atomic mass exist. For our $PbTiO_3$ structures on $SrTiO_3$, this indicates regions with more and less lead, or ideally: with and without lead. Combined with the SEM images taken in normal mode, this shows that the grains are connected to form chains of ferroelectric nanoparticles and that most chains are separated from each other.

$PbTiO_3$ crystallization

In order to study and control the crystallization of the amorphous $PbTiO_3$, we have performed XRD measurements as in Figure 6.4. The crystallinity of the thin film has been monitored as a function of temperature during and after the crystallization process, which shows the formation of almost exclusively (00L)-oriented $PbTiO_3$ around 550°C. Only a small fraction of (101)-oriented $PbTiO_3$ is present. The preferred (00L)-orientation implies that the crystallization of the $PbTiO_3$ layer is strongly influenced by the substrate. This observation supports the crystallization process as we described in section 6.2.2: The transfer of the P4VP morphology to the ex-situ annealed $PbTiO_3$, is most easily accomplished by preferential crystallization where the $PbTiO_3$ and the $SrTiO_3$ are in direct contact.

Furthermore, X-ray photoelectron spectroscopy (XPS) has shown that

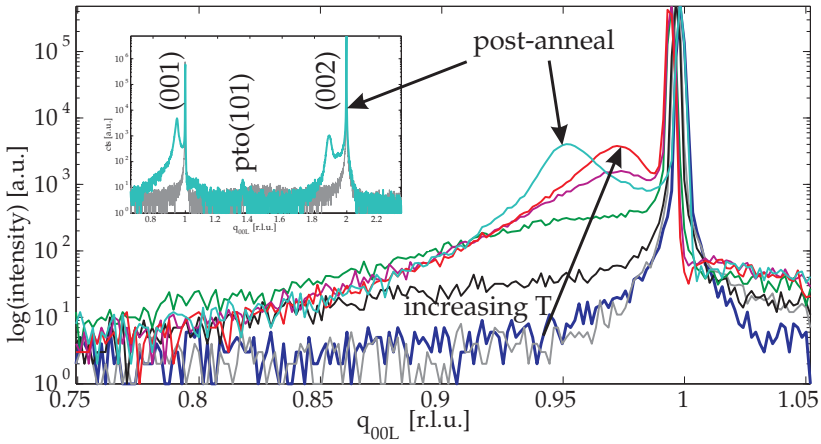

Figure 6.4: Temperature dependent X-ray diffractograms around the $SrTiO_3$(001) Bragg peak at 50; 300; 350; 500; 550; 600 and 50°C (the latter after annealing). The inset is an extended scan before and after annealing, which shows that the $PbTiO_3$ is mainly (00L)-oriented and partly (101)-oriented.

the top layers of the samples contain Pb, Ti, O and C. However, the amounts

of carbon are minute compared to the other elements, and can be explained by the presence of surface contamination as well as a negligible amount of residual carbon from incomplete degradation of the polymer. However, as the Pb, Ti and O peaks are not split, there is no sign of possible enclosure of this carbon in the $PbTiO_3$ structure.

Ferroelectric properties

The ferroelectric properties of the $PbTiO_3$ nanodots have been measured with piezoresponse-AFM. Due to the large roughness of the surface, we have not (yet) been able to obtain topographic images of the piezoresponse. Spectroscopy on single nanodots is successful as can be seen in Figure 6.5 and the nanoparticles exhibit ferroelectric behavior. Further measurements should provide more insight into the size and shape dependence of the ferroelectric response.

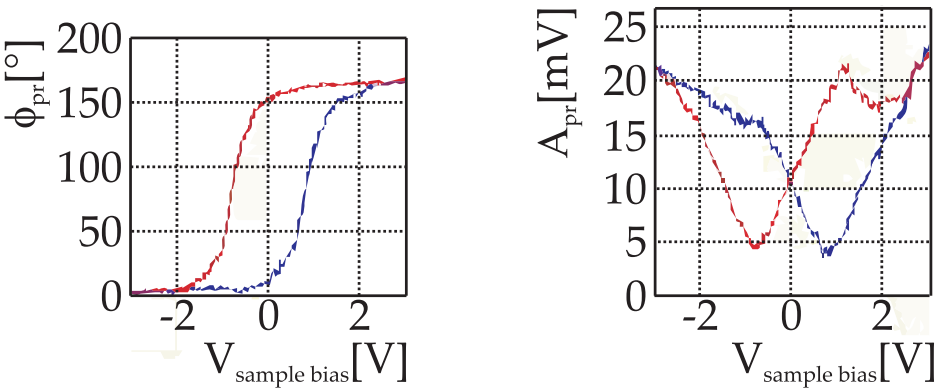

Figure 6.5: Piezoresponse phase ϕ_{pr} and amplitude A_{pr} measurements as a function of applied sample bias on a $PbTiO_3$ nanodot. Measured with $V_{dc} = 6V$; $V_{ac} = 3V$ and $f_{ac} = 45kHz$ (measurement by Anthony Ferri).

6.3 $PbTiO_3$ / $SrTiO_3$ superlattices

6.3.1 Introduction

The interest in superlattices of ferroelectric oxide perovskites has increased strongly since the proposition by the SONY research center of several ABO_3 superlattice structures for future oxide electronics [153]. Regarding PLD growth of these superlattices, the group of H. Christen was among the first to show the great atomic control of this method by growing three-color $BaTiO_3$ / $SrTiO_3$ / $CaTiO_3$ superlattices [154]. Besides these possible applications and the high atomic control that state-of-the-art growth methods offer, superlattices are also interesting from a theoretical point of view. One of the main interests is in the electrostatic coupling between the layers in an artificial dielectric/ferroelectric superlattice structure, in which the ferroelectric should induce polarization in the dielectric layer. The polarization and dielectric constant observed in $PbTiO_3/SrTiO_3$ superlattices are relatively high (P_s of the order of $10\mu C/cm^2$), ϵ_r of the order 10^2) [155]. Recently, it has been shown experimentally and confirmed theoretically that short-period $PbTiO_3/SrTiO_3$ superlattices (2 unit cells) are improper ferroelectrics, while superlattices with the same stoichiometry but a long period (12 unit cells), are proper ferroelectric [155]. This makes long-period superlattices ideal to study the induction of polarization by the ferroelectric in the dielectric. Since the dielectric constant of improper ferroelectrics is constant over a wide temperature range and is large in this specific case, these short-period superlattices are attractive for dielectric applications. The difference between the short- and long-period superlattices, illustrates the importance of the interfaces in these superlattices. We have grown $PbTiO_3/SrTiO_3$ superlattices with a relatively long period (~ 10 unit cells).

6.3.2 Experimental

For $PbTiO_3/SrTiO_3$ superlattices, the $PbTiO_3$ can be grown as described in the previous chapters. Although it has been shown that by using sputtering, $SrTiO_3$ can be grown in similar growth conditions as $PbTiO_3$ [156], using PLD, $SrTiO_3$ grown at 570°C and normal growth pressures ($pO_2 \approx 0.1$mbar) is likely to be oxygen deficient. On $PbTiO_3/SrTiO_3$ superlattices with $SrTiO_3$ grown at 570°C, we have only been able to measure leakage

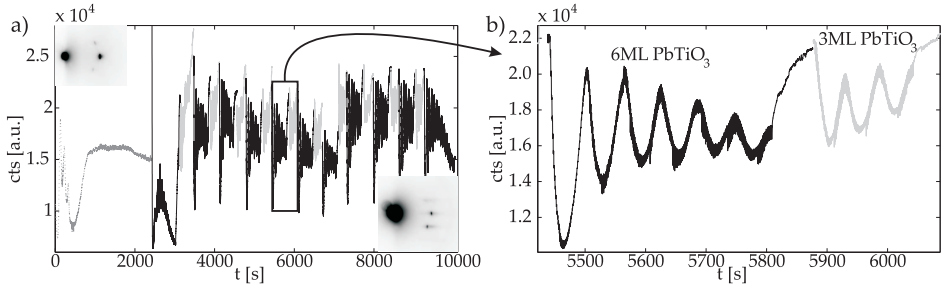

Figure 6.6: a) RHEED intensity profiles of a 10 periods 6ML $PbTiO_3$ (black), 3ML $SrTiO_3$ (gray) superlattice grown on $SrRuO_3$ (dotted gray) on $SrTiO_3$. Image (b) is a zoom of the 5th period. The insets in a) are the RHEED pattern before (left) and after (right) deposition.

currents. But growing $SrTiO_3$ at higher temperatures is problematic because it could lead to undesired lead loss from the $PbTiO_3$ layer. Therefore, we have grown $PbTiO_3$ and the first 1.5 monolayer of $SrTiO_3$ of every superlattice period using our typical $PbTiO_3$ growth parameters. The resulting $SrTiO_3$ capping layer should prevent lead loss and subsequently we have raised the temperature to 790°C to grow the remaining portion of the $SrTiO_3$ layer. This illustrates the high control of the growth at the atomic level that RHEED-assisted PLD allows. Figure 6.6 shows that for superlattices with the $SrTiO_3$ grown at 570°C, RHEED oscillations are observed for all layers, which is also the case for the split $SrTiO_3$ growth. Besides, good morphology with unit cell steps reflecting the substrate surface morphology, is shown by AFM on the resulting superlattice in Figure 6.7, confirming the layer-by-layer growth. The structural properties of these superlattices will be described in section 6.3.3 and the electrical characterization will be treated in section 6.3.3.

6.3.3 Results and discussion

Structural properties

The most important observation regarding the structural properties of the $PbTiO_3/SrTiO_3$ superlattices we have grown, is the low degree of intermixing of the superlattice layers. This is based on the large number of XRD su-

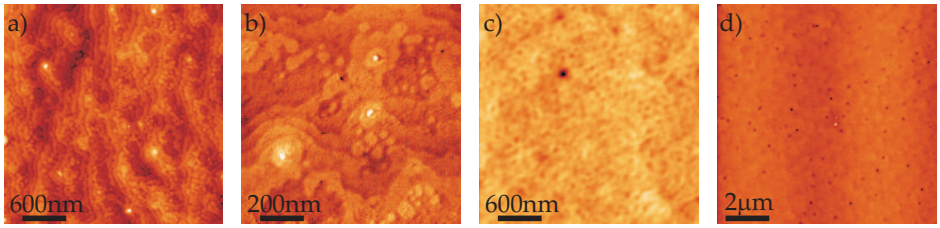

Figure 6.7: AFM images of the top surface of (a+b) a $(6PbTiO_3/3SrTiO_3)_{10}$ superlattice on $SrRuO_3$-electroded $SrTiO_3$ and a (c+d) a $(3PbTiO_3/3SrTiO_3)_{12}$ superlattice on $SrRuO_3$-electroded $DyScO_3$. The RMS roughness and full z-scale of these images are a) RMS= 3.4 Å, Δz= 4 nm; b) RMS= 4.4 Å, Δz= 4 nm; c) RMS= 1.7 Å, Δz= 3 nm; d) RMS= 3.6 Å, Δz= 9 nm.

perlattice peaks in Figure 6.8 and the sharp interfaces as observed in Figure 6.9. The number of superlattice peaks observed is considerably larger than for superlattices grown by rf-sputtering [141], which indicates less layer-intermixing. The amount of layer-intermixing is closer to that of MBE-grown superlattices [157]. Yet, one can argue whether this absence of intermixing is a positive aspect, since theoretical calculations [158] show that some degree of intermixing enhances the Pb off-centering and therefore the polarization of these superlattices.

The differences between the PLD growth method we have employed and the off-axis rf-sputtering technique used by Dawber et al. [156], could have large influence on the final material and, thus, the properties. Not only is the sputtering growth rate much slower and the growth temperature much lower (460°C versus our 570°C), but, maybe more importantly, at 460°C $PbTiO_3$ is grown in the tetragonal phase, whereas we grow it in the tetragonal phase but cycle it several times towards the cubic phase during the growth of the $SrTiO_3$ layers (based on our observations in chapter 4, we expect thin films of several unit cells thick to have a T_c above 800°C, so we do not actually reach the cubic phase). This thermal cycling could give rise to changes in the domain structure. Besides, there is a considerable risk of lead loss with our method, which could lead to deterioration of the ferroelectric properties of the $PbTiO_3$ layers.

However, this scenario is contradicted by the observations of the x-ray diffraction maps in Figure 6.10, which shows satellites similar to the ones ascribed in the previous chapters to the presence of 180° domains. Also in

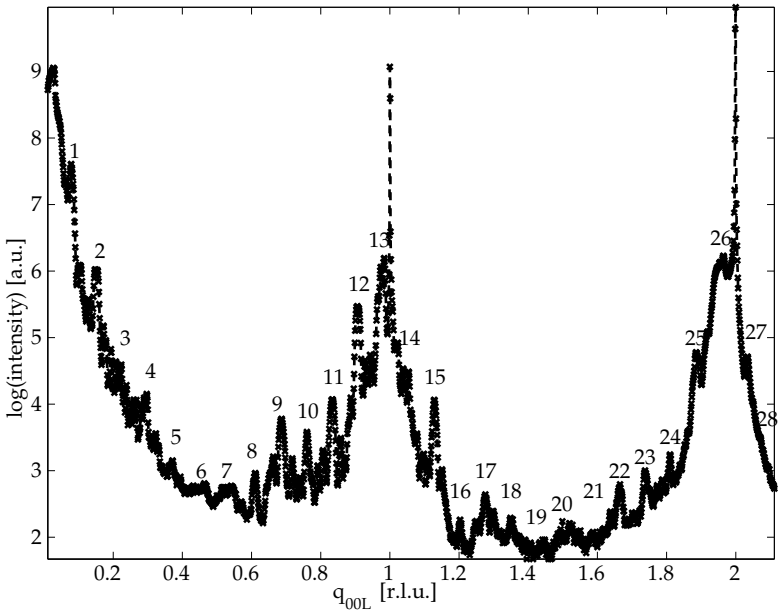

Figure 6.8: X-ray diffractogram along the (00L)-direction of a $(9PbTiO_3/4SrTiO_3)_6$ superlattice on 23 nm $SrRuO_3$ on $DyScO_3$. The superlattice peaks are indexed in line with the number of grown monolayers. Note that there is considerable interference between superlattice peaks and thickness fringes.

this case, the superlattice spacing is constant throughout diffraction orders, confirming that the superlattice is due to periodic domains. In this specific case of Figure 6.10, a $(9PbTiO_3/4SrTiO_3)_6$ superlattice, the in-plane modulation corresponds to a 66 Å periodicity of the domains. In general we have observed shorter domain periodicities for thinner $PbTiO_3$ layers. These observations do not only proof that the $PbTiO_3$ is ferroelectric, but also that the $SrTiO_3$ layers are non-conductive (electrical contact would cause short-circuiting, removing the driving force for 180° domain formation). It is, as far as we know, the first time that long-range periodic 180° patterns have been observed in ferroelectric superlattices. In conclusion, this means that the growth of $PbTiO_3/SrTiO_3$ superlattices has been achieved successfully by PLD. When the $SrTiO_3$ is grown at our typical $PbTiO_3$ growth temperature of 570°C, it is defect- and vacancy-rich, which gives rise to leakage currents. We believe that growing 1.5 monolayer $SrTiO_3$ after each $PbTiO_3$ layer at

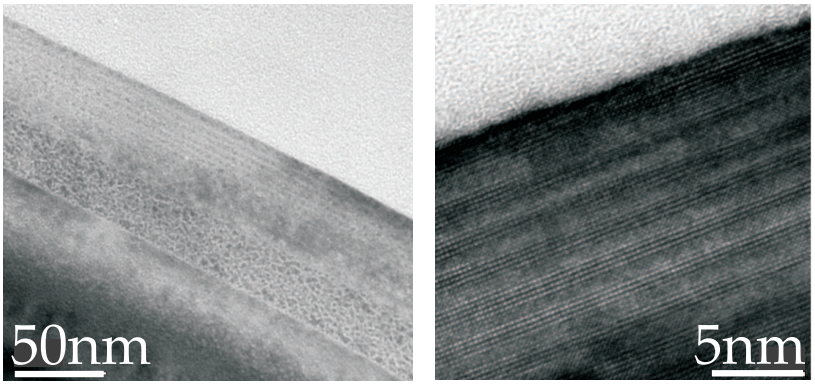

Figure 6.9: Bright field (a) and high resolution (b) TEM images of a $(6PbTiO_3/3SrTiO_3)_{10}$ superlattice on $SrRuO_3$-electroded $SrTiO_3$.

570°C as a capping layer and the subsequent $SrTiO_3$ at 790°C, has greatly reduced the number of defects and vacancies in the $SrTiO_3$. Whether we will be able to measure intrinsic properties of these superlattices, will depend on the stoichiometry of the superlattice and the electrode and interface quality.

Dielectric properties

Although we have been unable to measure macroscopic ferroelectric voltage-polarization hysteresis loops on superlattices of $PbTiO_3/SrTiO_3$ on $SrTiO_3$, we have performed impedance spectroscopy. A typical result on different electrodes on a single superlattice, is shown in Figure 6.11. This figure pinpoints the origin of the encountered problem for CV-measurements: The measurement is highly dependent on the electrode. While for some superlattices the measurement is dominated by extrinsic effects like grain boundary dipolar contributions, in other cases this is totally diminished and the intrinsic properties can be measured. Figure 6.11 shows measurements of the dielectric permittivity via different electrodes on a $(10PbTiO_3/4SrTiO_3)_6$ su-

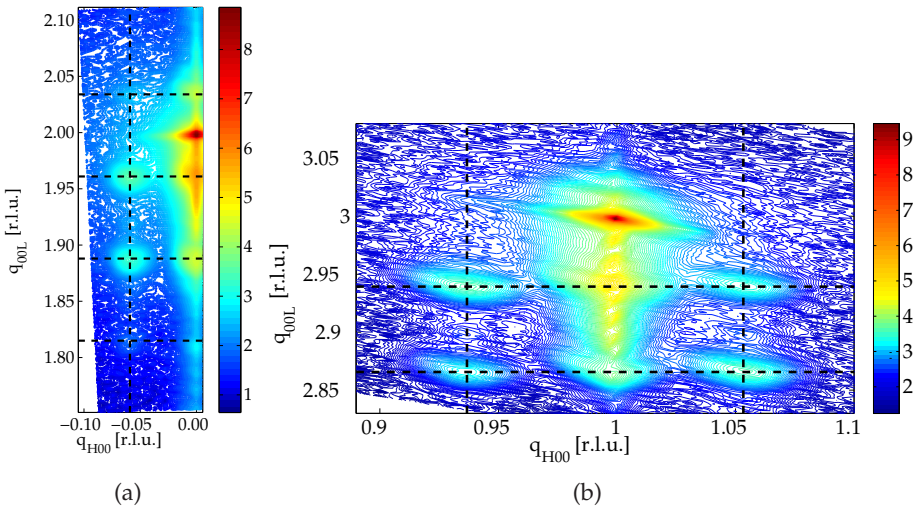

Figure 6.10: RSMs around the (a) (002) and (b) (103) Bragg peaks of a $(9PbTiO_3/4SrTiO_3)_6$ superlattice on $SrRuO_3$ on $SrTiO_3$.

perlattice. By plotting the imaginary part versus the real part of the dielectric permittivity (the so-called Cole-Cole plot), as shown in Figure 6.11(d,e), an intrinsic static dielectric constant $\epsilon(0) \approx 100$ can be extracted. This value is much lower than the $\epsilon(0) \sim 500$, which is observed in similar superlattices grown by sputtering [155, 159]. Remarkably, Stucki [159] shows that there is very little change in response for different frequencies in the range 10^3Hz$< f < 10^6$Hz, but this observation remains unexplained. They have only observed frequency dependence when the electrodes were of poor quality[1], but this should not influence the intrinsic dielectric constant and it is questionable which is the intrinsic value of the dielectric constant. Besides, this factor of 5 difference in the dielectric constant can be partly explained by the possible differences in intermixing between superlattices grown by PLD and sputtering [158]. Moreover, the PLD growth method that we have used can be unsuitable to grow this kind of superlattices, because Pb-loss during $SrTiO_3$ deposition can not be excluded.
The simulation of dielectric measurements is presented in Figure 6.11(d) and

[1]Private communication with Professor Matt Dawber, Stony Brook University (USA)

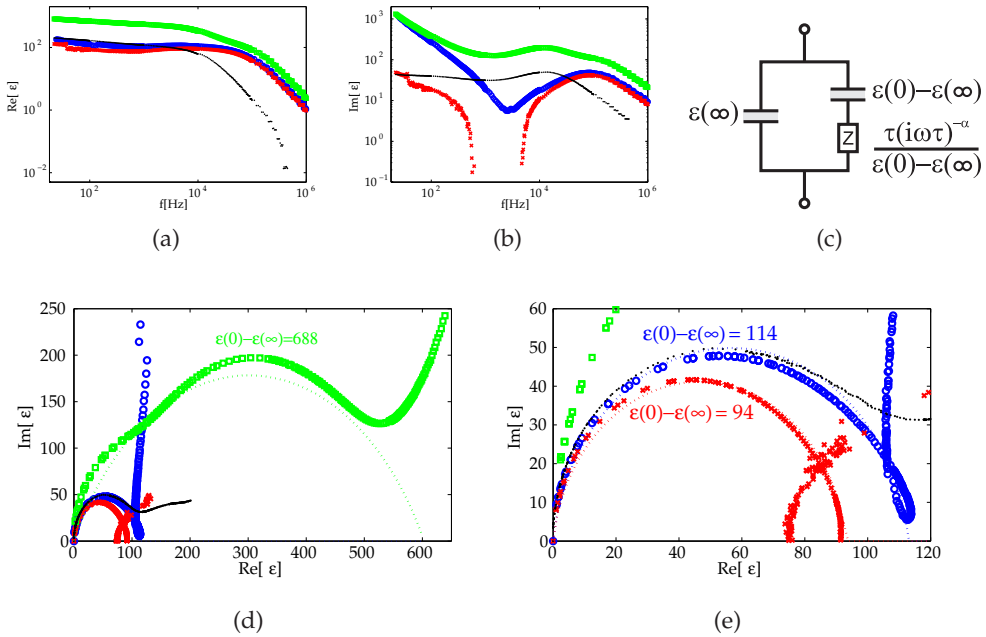

Figure 6.11: Real (a) and imaginary (b) part of the dielectric constant as a function of frequency measured on different electrodes and with driving amplitudes of 50 mV (green), 100 mV (black), 500 mV (red) and 1000 mV (blue) on a single $(9PbTiO_3/4SrTiO_3)_6$ superlattice. (c) The equivalent circuit used to simulate the Cole-Cole plots constructed from these measurements (c+d) indicates an intrinsic $\epsilon(0) \approx 100$, typically measured at 10^5Hz frequencies.

6.11(e) by dotted lines. The data are simulated using impedance spectroscopy with the equivalent circuit shown in Figure 6.11(c), as proposed by Cole and Cole [101] for dielectrics. Unlike many mechanisms used to explain dielectric absorption, which assume a purely dissipative element like a resistance in the equivalent circuit, the use of a complex impedance is more likely the actual behavior of dielectrics. This means that we use a complex impedance Z with a phase angle α which is independent of frequency. This α is very suitable to describe the behavior of dielectrics, since it implies a conservation of energy in the equivalent electrical circuit instead of a dissipation.

The phase angles and dielectric constants used to simulate the measure-

ments in Figure 6.11(d) are $\alpha = 3.6°$ and $\epsilon(0) - \epsilon(\infty) = 104 \pm 10$ for the high-frequency semicircle corresponding to the intrinsic response. The intermediate-frequency semicircle, corresponding to the extrinsic response due to grain boundaries, is simulated in Figure 6.11(e) with $\alpha = 14.4°$ and $\epsilon(0) - \epsilon(\infty) = 688$. The onset of a third semicircle at the lowest frequencies, is measured, which is probably linked to the response of the electrode/film interfaces. Especially for the intrinsic response, the parameter α is small, implying that the behavior is nearly that of an ideal Debye-like dielectric. All in all, this gives an intrinsic dielectric constant $\epsilon(0) = 104 \pm 10$. This is in close agreement to what is expected for a mixture of these two materials with a 9:4 $PbTiO_3 : SrTiO_3$ stoichiometry ($\epsilon = 138$ at room temperature, considering the dielectric constants of $PbTiO_3$ and $SrTiO_3$ at room temperature to be 66 and 300, respectively). Based on Landau theory, an enhancement of the dielectric constant is expected [159], which is only limited for the $PbTiO_3/SrTiO_3$ ratio of the current superlattice.

Finally, measurement of the intrinsic properties requires a frequency analysis and we show that, in our case, the intrinsic properties of the material only appear above ∼250kHz. Moreover, it is predicted and confirmed that the acoustic resonance frequency of these superlattices is determined by their periodicity and that this is in the order of 1GHz [160]. This makes them, in principle, suitable to be integrated with high speed electronics.

6.4 Conclusions

We have investigated the influence of size reduction of ferroelectric $PbTiO_3$ on its properties. This size reduction has been accomplished by fabricating nanodots via deposition on a substrate patterned with microphase separated block-copolymers and by growing superlattices of $PbTiO_3$ and $SrTiO_3$.
We have shown a successful method of using organic copolymers to obtain these ferroelectric chains of nanodots. Although a nanorod template of PS-b-P4VP is degraded at temperatures above $\sim 450°$C, capping the rods with $PbTiO_3$ and annealing at 565°C leads to ferroelectric chains of nanodots that crystallize above 500°C. In this way, the $PbTiO_3$ is both oriented by the substrate and structured by the polymer template. The obtained chains of nanodots can be used to examine the shape and size dependence of ferroelectrics at the nanoscale. In our case, no drastic changes in the ferroelectric proper-

ties have been observed by piezoresponse-AFM, as expected for nanodots of 30-60 nm.

The other route to size reduction we have followed, is growing superlattices of $PbTiO_3$ and $SrTiO_3$. These superlattices have been grown by PLD with non-conducting $SrTiO_3$ layers by depositing the first 1.5 monolayer of each $SrTiO_3$ layer at the $PbTiO_3$ growth temperature and the subsequent $SrTiO_3$ at 790°C. This results in structurally very good superlattices with very little layer intermixing as we can observe by XRD and TEM. The functional properties of these superlattices are not as good as those of the only group reporting in literature on the ferroelectric properties of $PbTiO_3/SrTiO_3$ superlattices [155].

In conclusion, we have not detected size effects in the nanodots of sizes ranging from 30-60 nm, which is in line with expectations, since theory predicts size effects below 6 nm [140]. Besides, we have grown superlattices with $PbTiO_3$ layers equal to or above the critical thickness for ferroelectricity. With only one reduced dimension, we do not expect nor observe any size effects in these superlattices. We do observe ferroelectric 180° domains by XRD in these superlattices, confirming their ferroelectricity. In addition, we have been able to deduce by impedance spectroscopy the intrinsic dielectric constant of a $(9PbTiO_3/4SrTiO_3)_6$ superlattice to be ~ 104. Therefore, the measured dielectric constant is independent of electrode or grain boundary effects. This value is not in line with earlier observations, but in close agreement with the value one would expect for a simple mixture of both components. This indicates that for superlattices with periods of 10-15 unit cells, grown by PLD, the material behaves bulk-like and interface effects do not play an important role.